

# ***Ab initio* molecular orbital study of the mechanism of photodissociation of *trans*-azomethane**

Ruifeng Liu,<sup>a)</sup> Qiang Cui, Kevin M. Dunn,<sup>b)</sup> and Keiji Morokuma  
Cherry L. Emerson Center for Scientific Computation, and Department of Chemistry, Emory University,  
Atlanta, Georgia 30322

(Received 5 September 1995; accepted 2 May 1996)

The mechanism of photodecomposition of *trans*-azomethane ( $\text{CH}_3\text{-N}=\text{N-CH}_3 \rightarrow 2\text{CH}_3\cdot + \text{N}_2$ ) has been investigated with high level *ab initio* molecular orbital calculations. Potential surfaces of the low-lying electronic states were explored by state-average complete active space self-consistent-field (sa-CASSCF) and multireference configuration interaction with single and double excitation (MRCISD) methods. The calculated vertical excitation energies for  $S_0 \rightarrow S_1$  and  $S_0 \rightarrow T_1$  transitions are in good agreement with experiments. The lowest crossing point between the  $S_0$  and  $S_1$  surfaces, around which excited molecules would make efficient internal conversion to the ground state, is found to be asymmetrical with a CNNC dihedral angle of  $92.8^\circ$  and two CNN angles of  $132.0^\circ$  and  $115.6^\circ$ , respectively. Transition structures for both simultaneous and sequential C–N bond cleavages on the  $S_0$  surface were found. Though the activation energy of sequential C–N bond cleavage is about 7 kcal/mol higher than that of the simultaneous C–N bond cleavage, the Gibbs free energy of activation is lower above  $0^\circ\text{C}$ , indicating that thermal decomposition of *trans*-azomethane is sequential. Photodissociation is expected to take place sequentially as well. In the sequential mechanism, dissociation of the first C–N bond on the  $S_0$  surface takes place endoergically without reverse barrier resulting in  $\text{CH}_3\text{N}_2$  intermediate, which should decompose almost immediately over a barrier of less than 1 kcal/mol. Thus, the photodissociation reaction is highly asynchronous but is nearly concerted. This mechanism can explain two seemingly contradictory photodissociation experiments that two methyl radicals have very different translational as well as internal energies and that the velocity vectors of the three fragments are strongly correlated. © 1996 American Institute of Physics. [S0021-9606(96)02230-1]

## **I. INTRODUCTION**

Photochemical as well as thermal decomposition of azoalkanes has been studied extensively for many years.<sup>1–3</sup> The excitation at the characteristic near-ultraviolet diffuse absorption band attributed to the  $S_0 \rightarrow S_1$  ( $n \rightarrow \pi^*$ ) transition<sup>4–6</sup> causes *cis*–*trans* isomerization in condensed phases. In the gas phase, however, the dominant process for acyclic azoalkanes is dissociation into alkyl radicals and nitrogen.<sup>7–8</sup> The photolytic decomposition of symmetric azoalkanes, has therefore, been used a viable source of alkyl radicals for kinetic, spectroscopic, and dynamics measurements.

Azomethane,  $\text{CH}_3\text{-N}=\text{N-CH}_3$  is the simplest among the symmetrical acyclic azoalkanes. As a prototype of acyclic azoalkanes, it has been the subject of many experimental investigations since the first report of its thermal and photodissociation more than 60 years ago.<sup>9</sup> The structural simplicity makes it a potential benchmark for understanding azoalkane photodissociation dynamics. Despite the large number of studies of azoalkane photochemistry, the electronic states involved and mechanism of photodissociation remain the subject of much speculation. For example, the ordering of

the low-lying electronic states of azomethane has not been firmly established. Although it has been accepted that the 350 nm photoexcitation corresponds to  $S_0 \rightarrow S_1$  transition, it remains unclear on which potential surfaces the photodissociation occurs. Another major question has been whether the two C–N bonds break in one kinetic step (concerted) or two (stepwise).<sup>10</sup> This question has been the subject of several state-of-the-art spectroscopic studies.<sup>11–14</sup> In the recent studies of Weisman *et al.*<sup>11,12</sup> using time-resolved coherent anti-Stokes Raman spectroscopy (CARS) technique, different appearance kinetics were observed for two internal quantum states of  $\text{CH}_3$ . It was concluded that each quantum state corresponds to a separate dissociation step, and photodissociation is therefore stepwise. However, a recent study using molecular beam photofragment translational spectroscopy, Lee *et al.*<sup>13</sup> observed that the angles between the asymptotic center-of-mass velocities for the two methyl radicals and nitrogen molecule were strongly correlated, implying the methyldiazanyl intermediate decomposes within a fraction of its rotational period. This observation suggests the photodissociation is a concerted one kinetic step reaction. Weitz *et al.*<sup>14</sup> have recently determined the translational, rotational, and vibrational distribution of the methyl fragment produced by UV photodissociation.

Since no decent modern *ab initio* molecular orbital (MO) method has been applied to study the potential surfaces of low-lying electronic states, the electronic states involved and

<sup>a)</sup>Present address: Department of Chemistry, East Tennessee State University, Johnson City, TN 37614.

<sup>b)</sup>Present address: Department of Chemistry, Hampden-Sydney College, Hampden-Sydney, VA 23943.

dissociation dynamics were interpreted with speculation and on the basis of an early single determinant semiempirical study of the low-lying electronic states of azomethane.<sup>15</sup> The semiempirical study predicted that at the ground-state geometry, ordering of the electronic states in increasing energy order is  $S_0$ ,  $T_1$ ,  $T_2$ , and  $S_1$ . With CNNC torsion, the  $S_0$  state increases energy,  $T_1$  decreases, and  $S_1$  changes slightly. At 90° dihedral angle, the  $T_1$  state is the lowest, and the  $S_0$  surface touches the  $S_1$  surface. As only a single determinant wave function was used in the semiempirical study, the predicted ordering of electronic states should not be considered reliable. For example, at 90° dihedral angle, the single determinant wave function is expected to give a rather bad description of the  $S_0$  state and give a too high energy. Experimentally<sup>6,16</sup> it has been found that the  $S_0 \rightarrow T_1$  excitation energy is much higher than that predicted by the semiempirical calculation,<sup>15</sup> casting doubts on whether the  $T_2$  surface is energetically accessible by 350 nm ultraviolet excitation.

While the present paper is being finalized,<sup>17</sup> a few *ab initio* studies on thermal decomposition of azomethane and methyldiazenyl radical ( $\text{CH}_3\text{N}_2$ ) were published. In these studies, both Hu and Schaefer<sup>18(a)</sup> and Andrews and Weisman<sup>19(a)</sup> located the transition structure of methyldiazenyl radical decomposition on the ground-state surface and found that there is a very small barrier for this process, implying methyldiazenyl has a very short lifetime. Hu and Schaefer<sup>18(b)</sup> also calculated vertical and adiabatic  $S_0 \rightarrow S_1$  and  $S_0 \rightarrow T_1$  excitation energies, and investigated the concerted and stepwise decomposition of azomethane on the ground-state potential surface with two-configuration SCF (TC-SCF). Based on their results of TC-SCF and TC-SCF-CISD calculation, they concluded that the synchronous decomposition of azomethane is not only energetically unfavorable but is an improbable reaction path.<sup>18(b)</sup> These conclusions are applicable to thermal decomposition, but may not be suitable for photodecomposition, because the photoreaction may not proceed on the ground-state surface and even if the excited molecules come back to the ground-state surface, they carry internal energy which is much higher than the activation barriers for bond breaking and unstatistically distributed, and therefore, the photodecomposition may not follow a minimum energy path.

Based on an RRKM study, Andrews has obtained the lifetime of the  $S_0$  state after excitation by 355 nm photon to be 20 ns, too long compared with the experimental lifetime of 1 ns, and thus, concluded that photodissociation of *trans*-azomethane on the  $S_0$  surface was highly improbable, suggesting  $T_1$  and  $T_2$  as the only surfaces on which the photodissociation occurs.<sup>19(b)</sup> This conclusion is oversimplified by assuming a statistical distribution of the excess energy. In photochemical reactions, in which the system crosses down from an excited to the ground-state with excess energies, one cannot assume statistical distribution. It depends on the dynamics of the reaction, and thus, on the characteristics of the potential energy surfaces on which the reaction takes place.

In the present study, we investigated molecular structures of azomethane and its potential surfaces of several low-

lying electronic states relevant to UV photodecomposition by *ab initio* complete active space self-consistent-field (CASSCF) and multireference configuration interaction with single and double excitation (MRCISD) methods. We calculated vertical excitation and ionization energies and explored the shapes of the potential surfaces accessible by 350 nm photoexcitation. Then, we determined the lowest point on the seam of crossing between  $S_0$  and  $S_1$  states and transition states for both simultaneous and sequential C–N bond dissociation. Finally, we present the overall potential energy profile for photodissociation and discuss the mechanism, its implication and comparison with recent experiments.

## II. COMPUTATIONAL APPROACH

Structures and potential surfaces around the equilibrium geometry are at first calculated with the CASSCF method<sup>20</sup> with an active space consisting of the bonding and antibonding  $\pi$  orbitals and the two lone pair orbitals on nitrogen atoms. Thus the CASSCF wave function is a linear combination of all configurations resulted from distributing six electrons in the four active orbitals [abbreviated as CASSCF(6,4)]. Molecular geometries of the lowest singlet and lowest triplet states of each symmetry under  $C_2$  point group are optimized by CASSCF(6,4) using the standard Huzinaga–Dunning double zeta plus polarization (DZP) basis set, i.e., [4s2p1d] contraction of a (9s5p1d) primitive set.<sup>21</sup> Potential surfaces with respect to CNNC torsion and CNN bending are explored by state-average (sa-)CASSCF/DZP<sup>22</sup> with equal weight for the lowest seven, four singlet and three triplet, states. Single and double C–N bond stretching potential curves are calculated by sa-CASSCF/DZP with larger active spaces. For single C–N bond stretching, the active space of CASSCF(6,4) is supplemented by a bonding and an antibonding C–N  $\sigma$  orbital [CASSCF(8,6)]. In the case of double C–N bond stretching, the other bonding and anti-bonding C–N  $\sigma$  orbital pair is also included in the active space [CASSCF(10,8)].

To obtain more reliable energetics, we carried out internally contracted MRCISD<sup>23</sup> calculation on top of the CASSCF(6,4) reference wave functions. For the MRCI calculations we adopted both the DZP and the correlation consistent valence triple zeta plus polarization (cc-pVTZ) basis set, i.e., [4s3p2d1f] contraction of a (10s5p2d1f) primitive set.<sup>24</sup> Molecular orbitals from both state-average (sa-) and state-specific (ss-) CASSCF(6,4) calculations were used in the MRCI calculation. The results are found to be very close to each other. For structures with only  $C_2$  symmetry, calculations using the full cc-pVTZ basis set are too large to be handled by the computers we use, we therefore used a truncated cc-pVTZ basis set excluding the *f* polarization functions on carbons and nitrogens and the *d* polarization functions on hydrogens.

Equilibrium and transition state structures of the simultaneous and sequential dissociation of *trans*-azomethane on the  $S_0$  and  $T_1$  surfaces are optimized by the MP2 method using the 6-31G\* (Ref. 25) and 6-311G(2d,p)<sup>26</sup> basis sets. Activation energies are recalculated by MP2, MP3,

MP4SDQ, QCISD, QCISD(T), CCSD, and CCSD(T) methods. Except for CCSD and CCSD(T), restricted and unrestricted versions of these methods were adopted for closed shell and open shell (doublet and triplet) states, respectively. For closed shell and open shell systems, CCSD and CCSD(T) are based on restricted Hartree–Fock and restricted open shell Hartree–Fock wave functions, respectively. For simultaneous dissociation on the  $S_0$  surface, the transition state is also optimized by CASSCF with an active space consisting of the bonding and antibonding  $\pi_{\text{NN}}$  and  $\sigma_{\text{CN}}$  orbitals [CASSCF(6,6)], and the activation energy is recalculated by MRCISD with the CASSCF(10,8) reference wave function. Frozen core approximation was used in all post Hartree–Fock calculations except CASSCF. The MP2, QCISD(T), CASSCF (for vibrational frequency only), and conical intersection calculations were carried out using the GAUSSIAN program packages,<sup>27</sup> and the CASSCF, CCSD(T), and MRCISD calculations were carried out using MOLPRO.<sup>28</sup>

### III. RESULTS AND DISCUSSION

#### A. Electronic and geometrical structures of the low-lying states of *trans*-azomethane

To understand the electronic structures of the low-lying electronic states of *trans*-azomethane, schematic molecular orbitals of the  $\pi$  and lone pair orbitals in the order of increasing orbital energy are given in Fig. 1. Dominant electron configurations of the lowest seven (four singlet and three triplet) states are given below, with the symmetry labels under  $C_{2h}$  point group.

$$S_0(^1A_g): \cdots (6b_u)^2(2a_u)^2(7a_g)^2$$

$$S_1(^1B_g) \& T_1(^3B_g): \cdots (6b_u)^2(2a_u)^2(7a_g)(2b_g)$$

$$S_2(^1A_u) \& T_3(^3A_u): \cdots (6b_u)(2a_u)^2(7a_g)^2(2b_g)$$

$$S_3(^1B_u) \& T_2(^3B_u): \cdots (6b_u)^2(2a_u)(7a_g)^2(2b_g).$$

The  $\pi^*$  orbital is empty in the ground state, but it is singly occupied in all the excited states listed above. Since the  $\pi^*$  orbital is antibonding with respect to the NN bond, one would expect an increase in the NN bond length on going from the ground to the excited states. One would also reasonably expect a softer torsional motion around the N–N bond in the excited states. The torsional motion will destroy the  $\sigma_h$  operation, so that the molecule may have only  $C_2$  symmetry in the excited states. Molecular structures of the lowest singlet and triplet states of each symmetry under  $C_2$  symmetry constraint are optimized by ss-CASSCF(6,4)/DZP. The results are given in Table I. Also given in this table, are energies calculated by CASSCF(6,4) and MRCISD with the CASSCF(6,4) reference wave function. For comparison, geometrical parameters of the ground state optimized by MP2 with the 6-311G(2d,2p) basis set are also given in this table. As the active space of the CASSCF calculations is quite small, only a small part of electron correlation was recovered by the CASSCF calculations. The MP2 calculations on the ground state, on the other hand, recovers a sig-

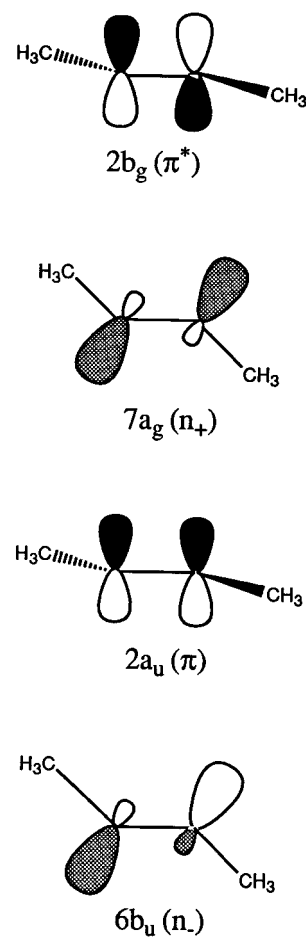


FIG. 1. Schematic  $\pi$  and lone pair orbitals of *trans*-azomethane.

nificant portion of electron correlation, and therefore, the MP2 structure was used in subsequent vertical excitation energy calculations.

As we can see in Table I, in agreement with expectation, the N–N bond lengths of the excited states are significantly longer than that of the ground state. The CNNC dihedral angles of the  $S_1$ ,  $T_1$ , and  $T_3$  ( $T_2$  structure was not optimized because this state has the same symmetry as  $T_1$ , which results in divergence ss-CASSCF calculation) calculated by CASSCF(6,4)/DZP are  $120.8^\circ$ ,  $97.1^\circ$ , and  $3.64^\circ$ , respectively. The energy differences between the excited and the ground states given in Table I correspond to adiabatic transition energies. For the  $S_0 \rightarrow S_1$  transition, the calculated result, 74.9 kcal/mol obtained from MRCISD plus Davidson size consistency correction [MRCISD(Q)], is in reasonable agreement with the observation that the onset of the  $n \rightarrow \pi^*$  band occurs at about 410 nm (69.8 kcal/mol).<sup>29</sup> For the  $S_0 \rightarrow T_1$  transition, Kuppermann *et al.*<sup>6</sup> observed a broad band from about 2.3 eV (53.0 kcal/mol) to 3.1 eV (71.5 kcal/mol) with a maximum at 2.75 eV. The lower limit, which corresponds to the adiabatic transition energy of this process, as well as another experimental result of 54 kcal/mol,<sup>16</sup> is also in good agreement with our calculated result, 51.4 kcal/mol.

TABLE I. Structural parameters<sup>a</sup> and energies<sup>b</sup> of the low-lying states of *trans*-azomethane calculated by ss-CASSCF(6,4)/DZP and MP2/6-311G(2*d*,2*p*) with C<sub>2</sub> symmetry restriction.

	ss-CASSCF(6,4)/DZP				MP2/6-311G(2 <i>d</i> ,2 <i>p</i> )
	S <sub>0</sub> ( <sup>1</sup> A <sub>g</sub> )	S <sub>1</sub> ( <sup>1</sup> B)	T <sub>1</sub> ( <sup>3</sup> B)	T <sub>3</sub> ( <sup>3</sup> A)	S <sub>0</sub> ( <sup>1</sup> A <sub>g</sub> )
R <sub>NN</sub>	1.240	1.266	1.302	1.444	1.253
R <sub>CN</sub>	1.454	1.449	1.457	1.437	1.464
R <sub>CH5</sub>	1.092	1.091	1.092	1.095	1.087
R <sub>CH6</sub>	1.092	1.092	1.092	1.092	1.087
R <sub>CH7</sub>	1.092	1.094	1.093	1.095	1.087
∠ <sub>NNC</sub>	113.2	124.9	116.9	119.4	111.7
∠ <sub>NCH5</sub>	112.2	110.2	112.8	113.0	111.6
∠ <sub>NCH6</sub>	108.2	110.1	108.8	105.2	107.9
∠ <sub>H5CH6</sub>	110.2	109.2	109.9	107.8	110.8
∠ <sub>H6CH7</sub>	107.7	108.2	107.8	108.0	107.6
∠ <sub>CNNC</sub> <sup>c</sup>	180.0	120.8	97.1	3.6	180.0
E <sub>CASSCF</sub>	-188.143 107	78.7	54.9	122.6	
E <sub>MRCISD</sub> <sup>d</sup>	-188.669 663	76.3	52.9	120.8	
E <sub>MRCISD(Q)</sub> <sup>e</sup>	-188.752 809	74.9	51.4	117.9	

<sup>a</sup>Numbering of atoms is given in Fig. 8. Bond lengths in Å and angles in degrees.

<sup>b</sup>Energy of the ground state is given in hartree, those of the excited states are given in kcal/mol relative to the ground state.

<sup>c</sup>Dihedral angle.

<sup>d</sup>Energy of internally contracted MRCISD with the CASSCF(6,4) reference wave function.

<sup>e</sup>Energy of internally contracted MRCISD plus Davidson size consistency correction.

## B. Vertical ionization potentials and vertical excitation energies of *trans*-azomethane

The photoelectron spectra of azomethane have been the subject of several experimental studies.<sup>30–33</sup> These studies established that the first three vertical ionization energies of *trans*-azomethane are 8.98, 11.84, and 12.3 eV. To compare with the experimental results, we made ss-CASSCF(6,4) and MRSDCI calculations on the neutral ground state and the lowest three doublet states of the cation using the DZP and cc-pVTZ basis sets. These calculations were carried out at the MP2/6-311G(2*d*,2*p*) structure of the ground-state *trans*-azomethane in Table I. The calculated ionization energies are compared with the experimental results in Table II. As is

TABLE II. Vertical ionization potentials of *trans*-azomethane.<sup>a</sup>

	<sup>1</sup> A <sub>g</sub> (neutral) <sup>b</sup>	<sup>2</sup> A <sub>g</sub>	<sup>2</sup> A <sub>u</sub>	<sup>2</sup> B <sub>u</sub>
DZP				
ss-CASSCF(6,4)	-188.142 488	7.98	11.45	12.06
MRCISD <sup>c</sup>	-188.669 625	8.57	11.87	12.36
MRCISD(Q) <sup>d</sup>	-188.753 106	8.72	11.90	12.35
cc-pVTZ				
ss-CASSCF(6,4)	-188.178 433	7.99	11.40	12.06
MRCISD	-188.819 514	8.73	11.96	12.52
MRCISD(Q)	-188.924 159	8.92	12.04	12.55
Exptl. <sup>e</sup>		8.98	11.84	12.3
Exptl. <sup>f</sup>		8.98	11.81	12.3

<sup>a</sup>In eV at the MP2/6-311G(2*d*,2*p*) structure of the ground-state neutral molecule.

<sup>b</sup>Energy of the ground-state *trans*-azomethane in hartrees.

<sup>c</sup>Internally contracted MRSDCI with the CASSCF(6,4) reference.

<sup>d</sup>Internally contracted MRSDCI with Davidson size consistency correction.

<sup>e</sup>Experimental results of Haselbach *et al.* (Ref. 31) and Houk *et al.* (Ref. 33).

<sup>f</sup>Experimental results of Robin *et al.* (Ref. 32).

shown in this table, the calculated results are in excellent agreement with experiments. The largest difference between the experimental and MRCISD results is 0.2 eV. The ss-CASSCF(6,4) calculation underestimates the first ionization potential, but gives very good results for the second and third ionization potentials.

Vertical excitation energies were also calculated by CASSCF(6,4) and contracted MRSDCI using the DZP and cc-pVTZ basis sets at the MP2/6-311G(2*d*,2*p*) ground-state geometry. As sa-CASSCF(6,4) method was used to explore the low-lying excited state potential surfaces, we did both ss- and sa-CASSCF-MRSDCI calculations to examine reliability of sa-CASSCF as an inexpensive approach to the excited state potential surfaces. The sa-CASSCF calculations included the lowest seven states, four singlet and three triplet, with equal weight. The natural orbitals obtained from sa-CASSCF(6,4) wave function were used in subsequent MRCISD calculations. The results are presented in Table III. As is shown in this table, the sa- and ss-CASSCF and MRCI give very similar results for most of the states. For the S<sub>1</sub> and T<sub>1</sub> states which are accessible by 350 nm (81.7 kcal/mol) photoexcitation, the excitation energies calculated by all the methods and two basis sets are almost the same, the largest variation is about 5 kcal/mol. For the S<sub>3</sub> state, variations between CASSCF and MRCI results are relatively large. However, this state is much higher compared to 350 nm photon energy, and therefore, it is not important for the present photochemistry.

From Table III, the vertical excitation energies, obtained by our best ss-MRCISD(Q)/cc-pVTZ method, are 87.0, 168.5, and 209.1 kcal/mol for transitions from S<sub>0</sub> to S<sub>1</sub>, S<sub>2</sub>, and S<sub>3</sub>, respectively, and 68.8, 115.7, and 162.5 kcal/mol for transitions from S<sub>0</sub> to T<sub>1</sub>, T<sub>2</sub>, and T<sub>3</sub>, respectively. The S<sub>0</sub>→S<sub>1</sub> transition in the gas phase was observed to have a

TABLE III. Vertical excitation energies of *trans*-azomethane by various methods and basis sets.<sup>a</sup>

	$S_0(^1A_g)^b$	$S_1(^1B_g)$	$S_2(^1A_u)$	$S_3(^1B_u)$	$T_1(^3B_g)$	$T_2(^3B_u)$	$T_3(^3A_u)$
sa- <sup>c</sup> /DZP							
CASSCF(6,4)	-188.132 121	87.6	165.0	288.8	69.5	107.0	159.1
MRCISD	-188.665 937	88.2	169.6	241.3	68.6	114.3	163.5
MRCISD(Q) <sup>d</sup>	-188.751 670	88.1	169.7	215.7	68.4	115.9	163.5
ss- <sup>e</sup> /DZP							
CASSCF(6,4)	-188.142 488	90.9	168.8	254.2	73.4	109.9	163.5
MRCISD	-188.669 625	89.4	170.7	225.2	70.3	115.6	164.6
MRCISD(Q)	-188.753 106	88.7	170.0	212.0	69.1	116.4	163.6
sa-cc-pVTZ							
CASSCF(6,4)	-188.167 435	87.8	165.1	287.1	70.0	107.0	159.4
MRCISD	-188.815 396	86.8	168.1	240.4	68.5	113.3	162.4
MRCISD(Q)	-188.922 540	86.4	168.2	214.9	68.1	115.0	162.4
ss-cc-pVTZ							
CASSCF(6,4)	-188.178 433	91.2	169.2	252.5	74.1	109.9	164.0
MRCISD	-188.819 514	88.1	169.4	223.1	70.3	114.8	163.7
MRCISD(Q)	-188.924 159	87.0	168.5	209.1	68.8	115.7	162.5
Exptl. <sup>f</sup>		83.9	155.7	219.1	63.4	111.6	

<sup>a</sup>In kcal/mol at the MP2/6-311G(2*d*,2*p*) geometry of the ground state.

<sup>b</sup>Energy of the ground state in hartrees.

<sup>c</sup>For sa-CASSCF, seven lowest states were included with equal weight. The CI calculations used the natural orbitals of the sa-CASSCF.

<sup>d</sup>With Davidson size consistency correction.

<sup>e</sup>State-specific CASSCF.

<sup>f</sup>Maximum absorption in the gas phase optical spectrum Ref. 4–6.

maximum at 3.64 eV (83.9 kcal/mol) in the optical spectrum,<sup>4,5</sup> which is in good agreement with the theoretical result. Another optical transition was observed<sup>5</sup> at about 6.75 eV (155.7 kcal/mol) and was confirmed<sup>6</sup> in the study of *trans*-azomethane electron impact excitation by differential electron scattering technique. It was assigned to a singlet→singlet transition. According to our calculations, it corresponds to the  $S_0$ → $S_2$  transition. Other observed<sup>6</sup> singlet→singlet transitions include one at  $9.5 \pm 0.1$  eV (219.1 kcal/mol) which corresponds well with the calculated result of the  $S_0$ → $S_3$  transition. Two singlet→triplet transitions have been observed to have maxima at 2.75 eV (63.4 kcal/mol) and 4.8 eV (110.7 kcal/mol), respectively, and were assigned to  $S_0$ → $T_1$  and  $S_0$ → $T_2$  transitions, respectively. This assignment was suggested to be incorrect by Steel *et al.*,<sup>15</sup> because in their semiempirical study, vertical excitation energies of the  $S_0$ → $T_1$  and  $S_0$ → $T_2$  transitions were calculated to be 45.5 and 67.5 kcal/mol, respectively. The good agreement between our calculated and experimental results confirms the original assignment of the electronic transitions. Another experimental study puts the vertical excitation energy at  $55.5 \pm 1.5$  kcal/mol.<sup>16</sup>

### C. Qualitative features of potential energy surfaces

For azoalkane compounds, most of the photochemistry studies were carried out using 350 nm photoexcitation. As we have shown, this photoexcitation corresponds to  $S_0$ → $S_1$  transition in *trans*-azomethane. The outcome of this photoexcitation in the gas phase is dissociation into nitrogen molecule and alkyl radicals, all in the ground state.<sup>14</sup> To understand the photodissociation kinetics and dynamics, one has to examine potential energy surfaces of the  $S_1$  and other nearby

states as well as the  $S_0$  state. Toward this goal, we applied sa-CASSCF/DZP method to the lowest seven states with equal weight. As we have shown that sa-CASSCF gives vertical excitation energies very close to the much more expensive MRCISD results, especially for the  $S_1$ ,  $T_1$ , and  $T_2$  states which might be involved in 350 nm photochemistry.

To explore the multidimensional potential surfaces, we at first keep most of the structural parameters at the MP2/6-311G(2*d*,2*p*) geometry of the ground state, and make CASSCF/DZP calculations varying some geometrical parameters. Figure 2 presents potential curves for simultaneous stretching of the two C–N bonds, maintaining  $C_{2h}$  symmetry, calculated by sa-CASSCF(10,8)/DZP with an active space consisting of the bonding and antibonding  $\pi_{NN}$  and  $\sigma_{CN}$  orbitals and the two lone pair orbitals on the nitrogen atoms. Shown in Fig. 3 are the potential curves for single C–N bond stretching, within  $C_s$  symmetry, at the sa-CASSCF(8,6)/DZP level with the active space consisting of the two lone pair orbitals, the bonding and antibonding  $\pi_{NN}$  orbitals, and the bonding and antibonding  $\sigma_{CN}$  orbitals of the breaking C–N bond. The 90 kcal/mol horizontal lines in these figures roughly suggest the energy range reachable with the photon plus thermal internal energy, corrected by  $\sim 4$  kcal/mol overestimation of the vertical excitation energy at this level of calculation, as discussed in Table III. These two figures indicate that, for either single or simultaneous double C–N bond breaking, only the  $S_0$  and  $T_2$  surfaces give the ground state products. On the  $S_0$  surface, there is a barrier at a C–N distance of about 2.1 Å for simultaneous double C–N bond breaking, but there is no reverse barrier for single C–N bond breaking. The  $S_0$ → $T_2$  transition, with its vertical excitation energy more than 30 kcal/mol higher

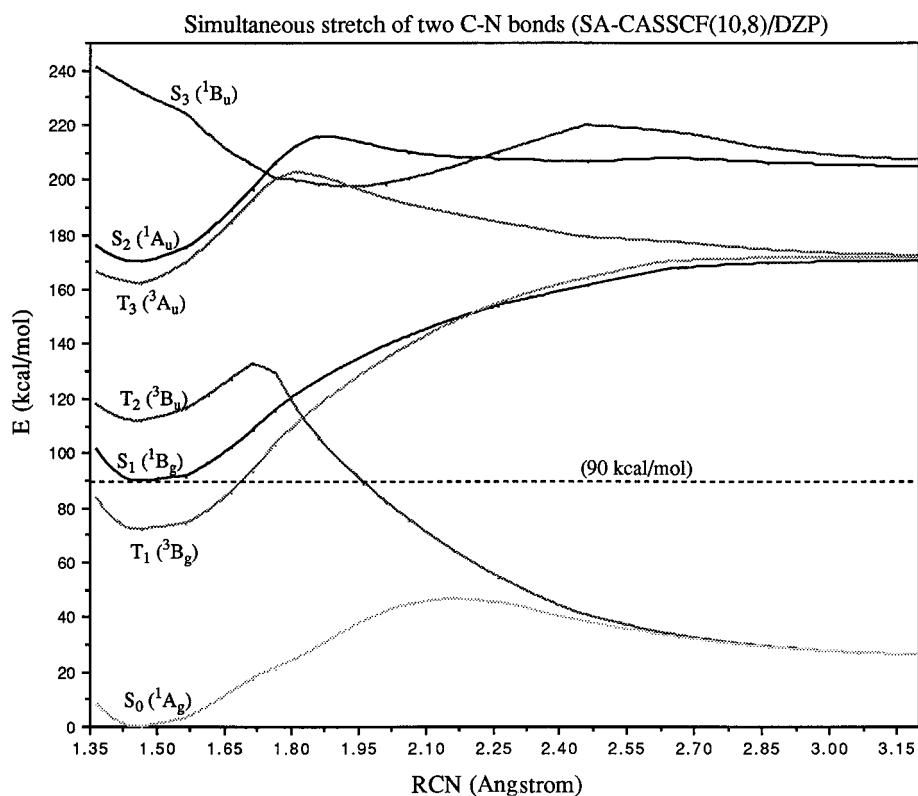


FIG. 2. Potential energy curves (in kcal/mol) of simultaneous stretch of two C–N bonds calculated by sa-CASSCF(10,8)/DZP. Other geometrical parameters were frozen at the MP2/6-311G(2d,2p) optimized geometry of the ground state.

than the 350 nm photon energy, is unlikely to initiate the photodissociation reaction. However, for both simultaneous and single C–N bond breaking, after a barrier at the C–N distance of about 1.8 Å the  $T_2$  surface crosses with  $S_1$  and

$T_1$ . Thus after the spin-forbidden  $S_0 \rightarrow T_1$  excitation, the system may make an internal conversion on the seam of crossing (or avoid crossing) from  $T_1$  to  $T_2$  and dissociate on the  $T_2$  surface resulting in ground-state products. Or after the

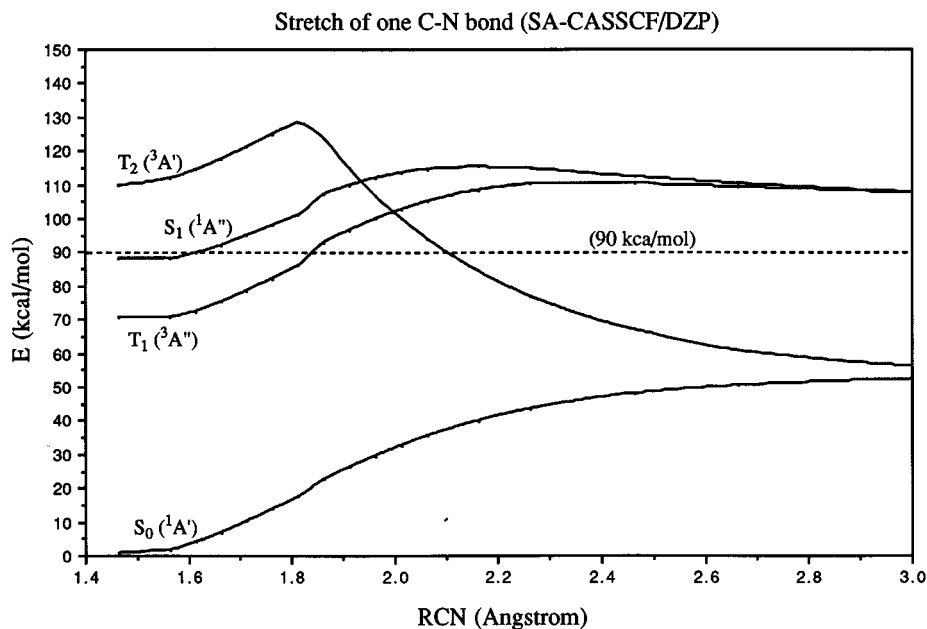


FIG. 3. Potential energy curves (in kcal/mol) of single C–N bond stretch calculated by sa-CASSCF(8,6)/DZP. Other geometrical parameters were frozen at the MP2/6-311G(2d,2p) optimized geometry of the ground state. For clarity, only the lowest four curves are given.

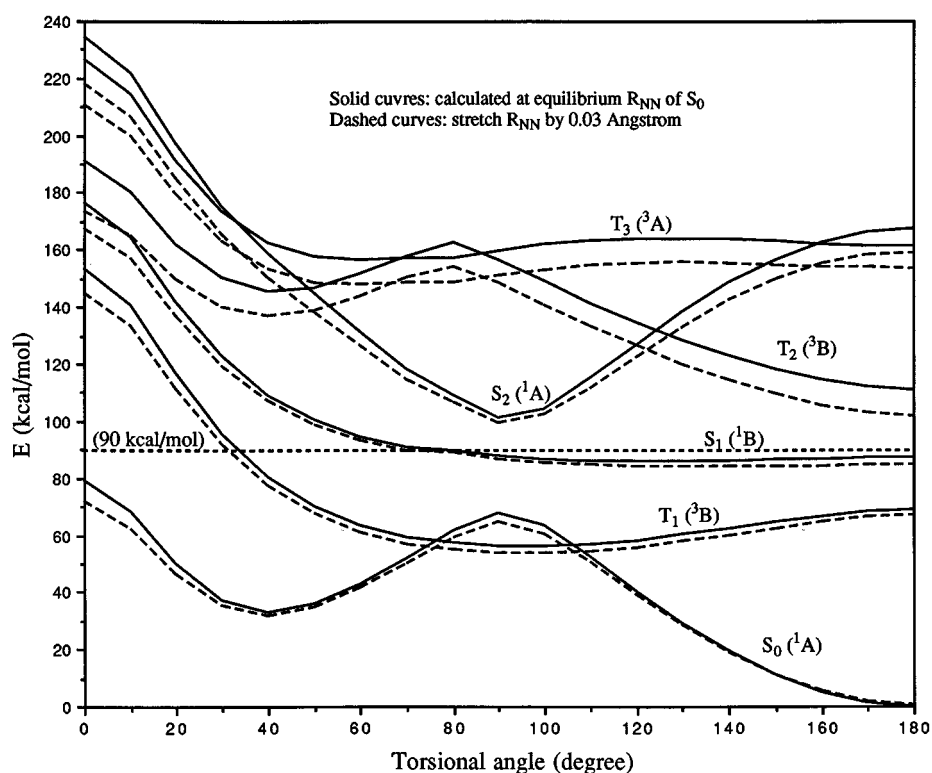


FIG. 4. CNNC torsional potential energy curves (in kcal/mol) calculated by sa-CASSCF(6,4)/DZP. For solid curves, other geometrical parameters were frozen at the MP2/6-311G(2*d*,2*p*) optimized geometry of the ground state, and for dashed curves the N–N distance was stretched by 0.03 Å.

$S_0 \rightarrow S_1$  excitation, the system may make an intersystem crossing on the seam from  $S_1$  to  $T_2$  and dissociate on the  $T_2$  surface. Because spin-forbidden transition and intersystem crossing, respectively, are involved, either of these processes would not be a major path of photodecomposition, if other more favorable paths exist.

The rate of internal conversion between the  $S_0$  and  $S_1$  states is roughly inversely proportional to the gap between the two surfaces, and for efficient internal conversion, the two surfaces must cross or weakly avoid crossing each other at an energy within the reachable energy. One would expect that internal rotation around the N–N bond and CNN bending bring the two singlet surfaces,  $S_0$  and  $S_1$ , close to each other, which would promote internal conversion from  $S_1$  to  $S_0$ . We calculated the CNNC torsional and CNN bending energy curves by sa-CASSCF(6,4)/DZP for the lowest seven states. Figure 4 presents the torsion curves calculated at the MP2/6-311G(2*d*,2*p*) equilibrium structure of the ground state and at the same structure but with a longer (by 0.03 Å) NN bond distance. This figure shows that  $S_1$  and  $T_1$  surfaces are very flat with torsional motion, and the ground state increases energy toward the perpendicular structure. At the perpendicular structure,  $S_1$  becomes the closest to  $S_0$ , about 20 kcal/mol higher. One notices that  $T_1$  is the ground-state here. Stretching NN distance lowers the energy of all the states around the perpendicular structure, but does not bring the  $S_1$  and  $S_0$  surfaces closer.

Figure 5 gives the symmetric CNN bending energy curves calculated at the MP2/6-311G(2*d*,2*p*) equilibrium

structure of the ground state. By increasing the CNN angle from the optimal angle of  $115^\circ$ – $125^\circ$  to  $180^\circ$ , the energy of both  $S_1$  and  $S_0$  states increases, and at the same time the gap between them decreases until the two states become degenerate at the linear structure. The linear structure however is too higher in energy for the 350 nm photon.

Combination of Figs. 4 and 5 suggests that  $S_1$  and  $S_0$  surfaces are likely to be close to each other within the 350 nm photon energy by simultaneous CNN opening and CNNC torsion. As shown in Fig. 6, we made additional torsional curve calculations at the MP2/6-311G(2*d*,2*p*) equilibrium structure but opening the CNN angle to  $140^\circ$ . This figure shows that the  $S_1$  surface nearly touches the  $S_0$  surface at a dihedral angle of  $100^\circ$ , at an energy which is below the 350 nm photon energy. This region seems to be reachable on the  $S_1$  surface from the Frank–Condon region without any barrier, and would provide an efficient “funnel” for nonadiabatic transition from the  $S_1$  state to the  $S_0$  state.

As most of the structural parameters were fixed at the ground-state geometry in the above figures and discussions of this subsection, the results can only be considered qualitative. To obtain more quantitative information on the potential energy surfaces, one has to optimize the structures of the critical points such as the transition states and crossing seam and calculate their energetics.

#### D. The lowest point on the $S_1$ – $S_0$ seam of crossing

We have at first determined the structure of the lowest point on the seam of crossing between  $S_1$  and  $S_0$ , the center

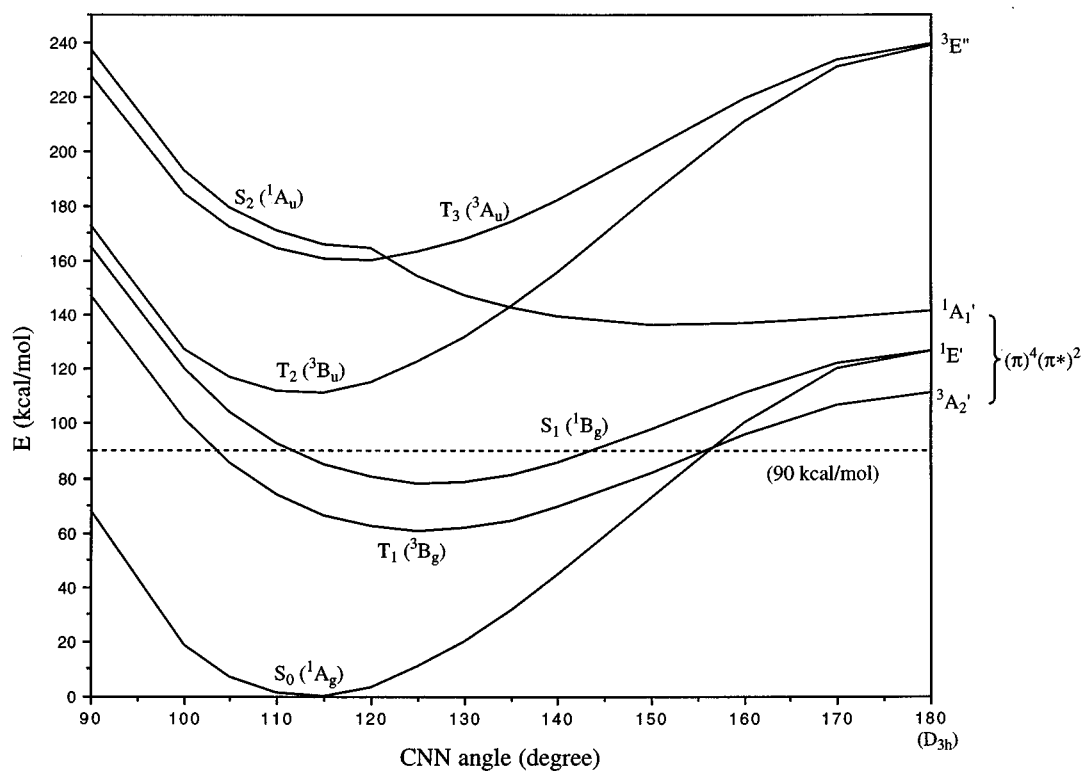


FIG. 5. CNN bending potential energy curves (in kcal/mol) calculated by sa-CASSCF(6,4)/DZP. Other geometrical parameters were frozen at the MP2/6-311G(2*d*,2*p*) optimized geometry of the ground state.

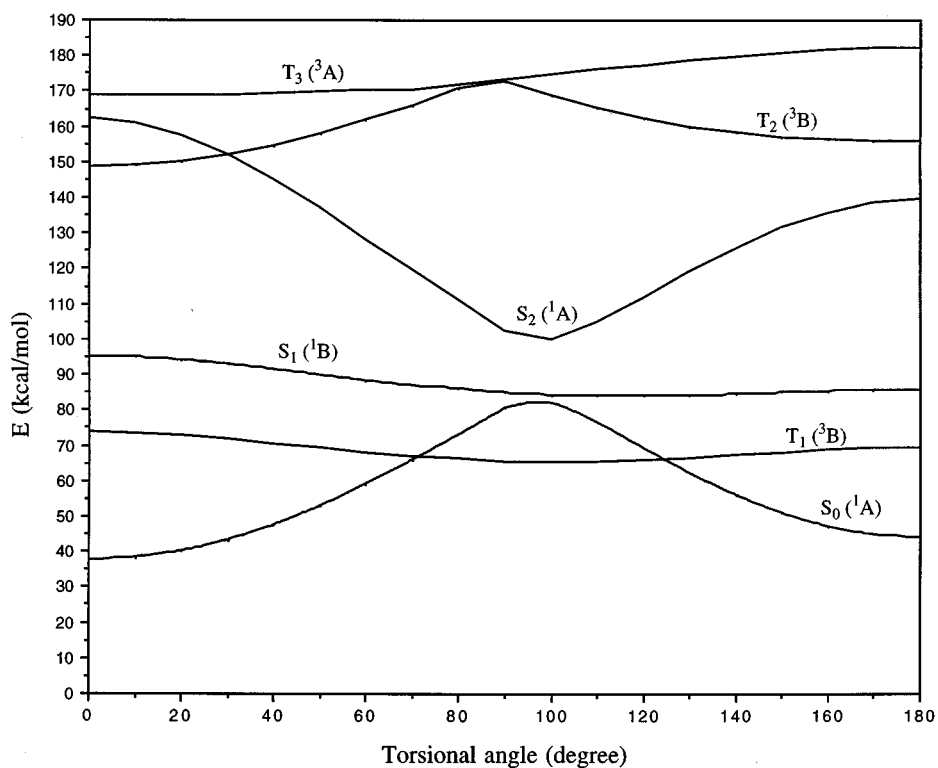


FIG. 6. CNN torsional potential energy curves (in kcal/mol) calculated by sa-CASSCF(6,4)/DZP. The two CNN angles were fixed at 140°, and other geometrical parameters were frozen at the MP2/6-311G(2*d*,2*p*) optimized geometry of the ground state.

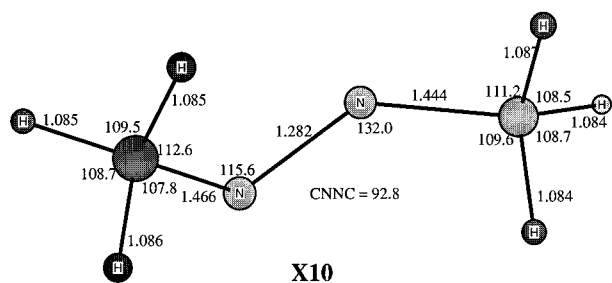


FIG. 7. Structure **X10** (in Å and deg) of the lowest point on the seam of crossing between the  $S_0$  and  $S_1$  surfaces located by sa-CASSCF(6,4)/DZP.

of the region where trajectories traveling on the  $S_1$  surface after 350 nm excitation will make a nonadiabatic transition to the ground state. Starting with the structure suggested in Fig. 6, we made extensive sa-CASSCF(6,4)/DZP conical intersection calculations using GAUSSIAN 94. It turns out convergence of this geometry optimization with GAUSSIAN 94 is very slow, probably due to very flat potential surface along the torsional coordinates around the perpendicular heavy atom configuration. Several eigenvalues of the updated Hessian are very close to zero making the calculations jump back and forth in the torsional coordinates without decreasing gradients in other directions. To overcome this problem, we first fixed the torsional coordinates and optimized the rest of the internal coordinates. When the gradients along these coordinates are sufficiently small, the torsional coordinates were unfrozen. The final optimized structure (**X10**) of the lowest crossing point between  $S_0$  and  $S_1$  is shown in Fig. 7. A prominent feature of this structure is that it is highly asymmetrical, i.e., the two CNN angles are  $132.0^\circ$  and  $115.6^\circ$ , respectively. The two CN bond lengths are 1.466 and 1.444 Å, respectively. The CNNC dihedral angle is  $92.8^\circ$ , indicating the two CN bonds are nearly perpendicular to each other. At **X10**, the sa-CASSCF(6,4)/DZP energy difference between  $S_1$  and  $S_0$  is 0.037 mhartree, and the  $S_1$  state is 73.8, 72.0, and 70.5 kcal/mol higher than the ground-state equilibrium at sa-CASSCF(6,4)/DZP, MRCISD/DZP, and MRCISD(Q)/DZP levels of theory. Considering the  $S_0 \rightarrow S_1$  vertical excitation energy calculated by MRCISD(Q)/DZP is 88.1 kcal/mol, **X10** is easily accessible from the Franck-Condon structure, and internal conversion of the excited azomethane is expected to be quite efficient. One would note, that since the structure **X10** has a CNNC dihedral angle of  $93^\circ$ , the decomposition of *cis*-azomethane upon  $S_0 \rightarrow S_1$  excitation would react qualitatively in the same way as *trans*-azomethane.

Starting from **X10**, we followed the meta-intrinsic reaction coordinate (IRC), i.e., the minimum energy path with the mass weighted Cartesian coordinate, on  $S_0$  surface at the MP2 level of theory. It is found that the meta-IRC calculation leads to *cis*-azomethane. This is consistent with the experimental finding that in condensed phase, UV irradiation of azoalkanes results in *cis-trans* isomerization. The excess energy of the excited molecule is perhaps carried away by intermolecular collisions in the condensed phases. Though a dynamics calculation will be required for any quantitative

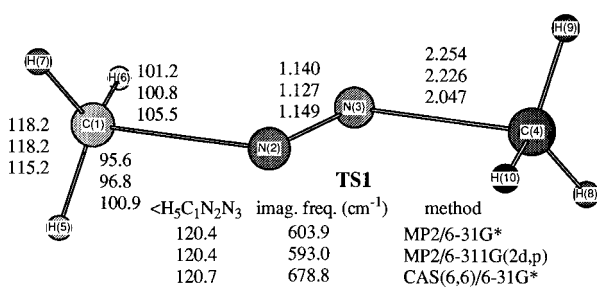


FIG. 8. Transition state structure **TS1** (in Å and deg) of simultaneous C–N bond dissociation on the  $S_0$  surface, determined with three different methods. Only symmetry unique geometry parameters are given in the  $C_{2h}$  symmetry.

discussion, this feature of the potential surface suggests that, in the gas phase the system with excess energy will not proceed directly to dissociate but will spend some time as a ground-state molecule with unstatistically distributed internal excitation, before finding its way to the C–N bond dissociation on the ground-state surface. This picture is consistent with the experiment that the lifetime of the first dissociation step is about 1 ns, not as long as the statistical rate lifetime of 10–20 ns but not as short as the direct dissociation lifetime of ps range.

## E. Transition states and energetics on the $S_0$ surface

After the nonadiabatic transition in the vicinity of **X10**, trajectories will travel on the ground potential surface  $S_0$ . To locate the transition state on  $S_0$  for simultaneous dissociation of two C–N bonds, we made RMP2 and CASSCF transition state geometry optimization. As shown in Fig. 8, MP2 calculations using both the 6-31G\* and 6-311G(2d,p) basis sets located a stationary structure **TS1** with the C–N distance of 2.253 and 2.226 Å, respectively. Vibrational analysis gives only one imaginary frequency for the symmetric C–N stretching mode, indicating it is indeed the transition state for simultaneous dissociation of two C–N bonds. The lowest antisymmetric frequencies are 139 and  $145\text{ cm}^{-1}$  for 6-31G\* and 6-311G(2d,p), respectively, for C–N stretch, consistent with the fact that this is a very loose transition state with long C–N distances. We have also determined the transition state with the CASSCF(6,6)/6-31G\* method, with an active space consisting of the bonding and antibonding  $\pi_{NN}$  and  $\sigma_{CN}$  orbitals. The structure obtained, also shown in Fig. 8, has a C–N distance of 2.047 Å and an antisymmetric C–N stretching frequency of  $177\text{ cm}^{-1}$ . The structures of **TS1** are consistent with the qualitative feature of Fig. 2. The differences between the MP2 and CASSCF structures are small, except for the C–N distances which are larger by 0.2 Å in the MP2 structure than in the CASSCF structure. It is probably worth mentioning that RHF/6-31G\* transition state optimization led to dissociation, indicating that the dissociation is simply uphill, an expected failure of the RHF method to describe this process.

The simultaneous C–N bond dissociation of azomethane on the  $S_0$  surface was studied recently by Hu and Schaefer.<sup>18</sup>

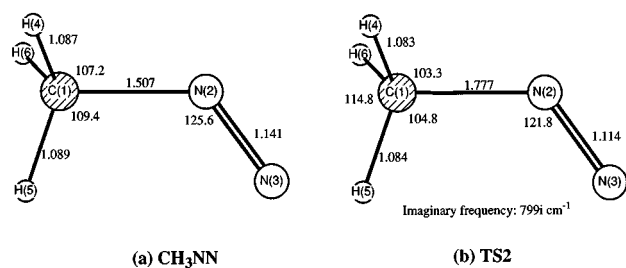


FIG. 9. (a) Ground ( ${}^2A'$ ) state equilibrium and (b) C–N bond dissociation transition state structure **TS2** (in Å and deg) of methyl diazenyl radical optimized by UMP2/6-311G(2*d,p*).

Using TCSCF/DZP and TCSCF/TZ2P, they found there is no transition structure for simultaneous dissociation and concluded that synchronous decomposition of azomethane is not only energetically unfavorable but is an improbable reaction path. This is different from our results, and the difference may be attributed to the fact that a TC-SCF wave function is insufficient for a proper description of the simultaneous breaking of two C–N bonds coupled with shrinking of the N–N bond.

We also searched for transition state of single C–N bond cleavage with RMP2, QCISD, and CASSCF(8,6), with the active space consisting of the two lone pair orbitals on nitrogen atoms, the bonding and antibonding  $\pi_{\text{NN}}$  orbitals, and the bonding and antibonding  $\sigma_{\text{CN}}$  orbitals of the breaking C–N bond, in conjunction with the 6-31G\* basis set. It is found that the dissociation is uphill without reverse barrier, in agreement with the features shown in Fig. 3. The ground-state structure of the dissociation product, methyl diazenyl radical ( $\text{CH}_3\text{N}_2$ ), optimized by UMP2/6-311G(2*d,p*) is shown in Fig. 9(a). The transition state **TS2** for cleavage of

the remaining C–N bond from  $\text{CH}_3\text{N}_2$  obtained by UMP2/6-311G(2*d,p*) is presented in Fig. 9(b).

Energetics for both simultaneous and sequential dissociation of *trans*-azomethane on the  $S_0$  surface calculated by different theoretical methods are shown in Table IV. All the energy calculations were carried out at the MP2 optimized structures. Usually the optimized structures are not very sensitive to the higher level correlation effect, and the MP2 optimization is considered to be sufficient for reliable energetics. For most of the species, the relative energies calculated by MP4SDQ, QCISD, and QCISD(T) are very close, differing by less than 4 kcal/mol. One exception to this is the relative energy of the transition state for simultaneous C–N dissociation, **TS1**. For this structure, the energies calculated by RMP2, RMP3, RMP4SDQ, and QCISD are about 70 kcal/mol higher than the reactant, but perturbative triple excitation has a large effect on the relative QCISD energy and results in a relative QCISD(T) energy 18 kcal/mol lower than that of QCISD. As shown also in Table IV, perturbative triple excitation has a similarly large effect on the coupled cluster energies. Such a large effect of triple excitation on relative energy is not very common. In order to ascertain the activation barrier of this dissociation channel, we have carried out internally contracted MRCISD calculation, with the CASSCF(10,8) reference wave function. With the DZP basis set, the CI wave function is a linear combination of 1.6 million contracted configurations, with the number of uncontracted configurations of 54 million. The activation energy obtained from MRCISD without and with Davidson size consistency correction are 55.2 and 58.0 kcal/mol, respectively. For **TS2**+ $\text{CH}_3$ , similar MRCISD(Q) calculation was unsuccessful because of too many contracted configurations for the low symmetry system. At the CCSD(T)/cc-pVTZ

TABLE IV. Energetics (in kcal/mol)<sup>a</sup> of simultaneous and sequential dissociation of *trans*-azomethane at MP2/6-311G(2*d,p*) optimized structures on the ground-state potential surface ( $S_0$ ).

Method	Reactant <sup>b</sup>	Simultaneous <b>TS1</b>	Sequential		
			$\text{CH}_3\text{N}_2 + \text{CH}_3$	<b>TS2</b> + $\text{CH}_3$	$\text{N}_2 + 2\text{CH}_3$
MP2/6-311G(2 <i>d,p</i> ) <sup>c</sup>	−188.803 386	68.5(60.5)	63.7(58.3)	68.9(61.2)	34.8(22.8)
MP3/6-311G(2 <i>d,p</i> ) <sup>c</sup>	−188.828 696	74.3(66.3)	57.9(52.5)	63.2(55.5)	34.1(22.1)
MP4SDQ/6-311G(2 <i>d,p</i> ) <sup>c</sup>	−188.838 618	71.3(63.3)	56.3(50.9)	60.2(52.5)	30.4(18.4)
QCISD/6-311G(2 <i>d,p</i> ) <sup>c</sup>	−188.839 252	70.2(62.2)	53.8(48.4)	56.9(49.2)	30.5(18.5)
QCISD(T)/6-311G(2 <i>d,p</i> ) <sup>c</sup>	−188.868 970	52.2(44.2)	56.9(51.5)	59.5(51.8)	34.2(22.2)
CCSD/DZP <sup>d</sup>	−188.749 874	77.0(69.0)	59.6(54.2)	65.9(58.2)	36.0(24.0)
CCSD(T)/DZP <sup>d</sup>	−188.771 377	58.6(50.6)	61.3(56.3)	67.1(59.4)	39.0(27.0)
CCSD/cc-pVTZ <sup>d,e</sup>	−188.857 823	71.9(63.9)	54.8(49.4)	58.5(50.8)	29.5(17.5)
CCSD(T)/cc-pVTZ <sup>d,e</sup>	−188.889 554	53.2(45.2)	57.4(52.0)	60.0(52.2)	33.0(21.0)
MRCISD/DZP <sup>f</sup>	−188.687 044	55.2(47.2)			
MRCISD(Q)/DZP <sup>f</sup>	−188.759 523	58.0(50.0)			

<sup>a</sup>Numbers in parentheses are relative energies with zero-point vibrational energy corrections. The latter are estimated from MP2/6-311G(2*d,p*) frequencies scaled by 0.93.

<sup>b</sup>Total energy in hartrees calculated at the MP2/6-311G(2*d,p*) equilibrium structure.

<sup>c</sup>Restricted (*R*-) and unrestricted (*U*-) MP and QCI methods for closed shell and open shell species, respectively.

<sup>d</sup>Restricted CCSD method for both closed shell and open shell species.

<sup>e</sup>Without *f* polarization functions on carbons and nitrogens and *d* polarization functions on hydrogens.

<sup>f</sup>With the CASSCF(10,8) reference wave function.

level of theory, the activation barriers for simultaneous and sequential C–N cleavage are 53.2 and 60.0 kcal/mol. Taking into account zero-point vibrational energy correction [estimated by MP2/6-311G(2*d*,*p*) frequencies scaled by 0.93], the barrier heights for simultaneous and sequential C–N bond dissociation are 45.2 and 52.2 kcal/mol, respectively, indicating simultaneous C–N dissociation is favored by thermal decomposition from activation energy considerations.

For the sequential dissociation mechanism, the C–N bond dissociation energy ( $D_e$ ) for *trans*-azomethane  $\rightarrow$  CH<sub>3</sub>N<sub>2</sub> + CH<sub>3</sub> calculated by different methods ranges from 63.7 to 53.8 kcal/mol, as also shown in Table IV. After zero-point vibrational energy correction, the dissociation energy  $D_0$  obtained by QCISD(T)/6-311G(2*d*,*p*) and CCSD(T)/cc-pVTZ is 51.5 and 52.0 kcal/mol, respectively. This  $D_0$  agrees very well with the experimental result, 51.2 kcal/mol, reported by Steel *et al.*<sup>34</sup> The transition state energy of the C–N bond cleavage of methyldiazenyl radical, **TS2**, plus CH<sub>3</sub>, is calculated to be 59.5 [QCISD(T)] and 60.0 kcal/mol [CCSD(T)] higher than the reactant *trans*-azomethane, indicating that the transition state, **TS2**, is only 2.6 kcal/mol higher than the methyldiazenyl intermediate. Taking into account zero-point correction, the activation energy for the C–N bond cleavage in methyldiazenyl radical is only 0.2 kcal/mol. This indicates that methyldiazenyl radical is very unstable and should have a very short lifetime. The overall barrier height with zero-point correction for sequential decomposition of *trans*-azomethane is 51.8 and 52.2 kcal/mol at the QCISD(T) and CCSD(T) levels of theory, respectively.

As the activation barrier of simultaneous decomposition (45.2 kcal/mol as calculated by CCSD(T)/cc-pVTZ) is calculated to be 7.0 kcal/mol lower than the sequential decomposition, it seems the simultaneous pathway is favored for thermal decomposition. However, sequential decomposition is strongly favored by entropy consideration. The entropies calculated at 298 K from the scaled MP2/6-311G(2*d*,*p*) frequencies are 83.9, 63.3, 65.5, and 46.8 cal(mol K)<sup>-1</sup> for **TS1**, methyldiazenyl radical, **TS2**, and CH<sub>3</sub> radical, respectively. The entropy difference of the transition states of the sequential and simultaneous decomposition is, therefore, 28.4 cal(mol K)<sup>-1</sup>, favoring sequential decomposition. With this large entropy difference, the free energy of activation for sequential decomposition is lower than for simultaneous decomposition by 0.8 kcal/mol at 273 K and by 3.6 kcal/mol at 373 K. Therefore, considering the free energy of activation, sequential decomposition of *trans*-azomethane is favored at temperatures above 0 °C.

## F. Transition states and energetics on the $T_1$ surface

As we discussed above, decomposition on the triplet surface is less likely, because it involves a weaker  $S_0 \rightarrow T_1$  excitation or spin-forbidden  $S_1 \rightarrow$  triplet intersystem crossing in the presence of a more efficient  $S_1 \rightarrow S_0$  internal conversion pathway. Nevertheless, such a possibility exists<sup>19</sup> and we calculated transition structure and energy for decomposition on the lowest triplet surface. As expected from the feature of  $T_1$

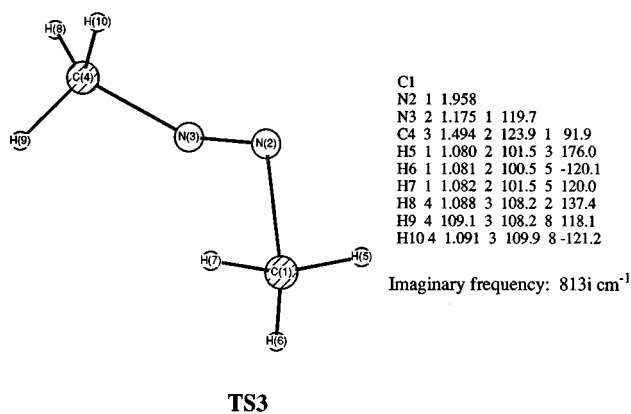


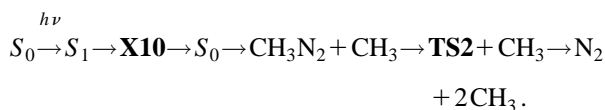
FIG. 10. Transition state structure **TS3** (in Å and deg) of sequential C–N bond dissociation on the  $T_1$  surface optimized by UMP2/6-311G(2*d*,*p*).

dissociation curve shown in Fig. 2, transition state search for simultaneous C–N bond cleavage on the  $T_1$  surface with UMP2/6-31G\* method resulted in breaking of the C–N bonds with a significant increase in energy to produce excited state products. This indicates simultaneous decomposition on  $T_1$  surface is an improbable reaction path.

The  $T_1$  surface crosses with  $T_2$  in  $C_s$  symmetry, as shown in Fig. 3. By reducing the symmetry, a transition state is expected to arise from avoid crossing between  $T_1$  and  $T_2$  and leads to the ground-state product. Optimization by UMP2/6-311G(2*d*,*p*) without symmetry on the lowest triplet surface located a transition structure **TS3** shown in Fig. 10. Vibrational analysis indicates there is only one imaginary frequency which corresponds to the single C–N bond cleavage. IRC calculation with a smaller basis set confirms that dissociation from this transition state gives the ground state product. At the QCISD(T)/6-311G(2*d*,*p*) level, the energy of **TS3** relative to the ground state equilibrium is 66.0 and 62.1 kcal/mol without and with zero-point correction, respectively. This is more than 10 kcal/mol higher than the transition states for both simultaneous and sequential decomposition on the  $S_0$  surface.

## G. The overall potential energy profile

Combining all the findings in the preceding subsections, we can construct an overall potential energy profile for photodissociation of *trans*-azomethane, as shown in Fig. 11. One can envision the most probable path of 350 nm photodecomposition as follows:



After UV excitation, the system will travel on the  $S_1$  potential surface until it reaches the region of  $S_0$ – $S_1$  crossing **X10**, which would be easily accomplished by NCCN torsion accompanied by asymmetrical CNN bending. Here the system will make a nonadiabatic transition to the ground-state  $S_0$ . Since the energy gradient vector at **X10** takes the system

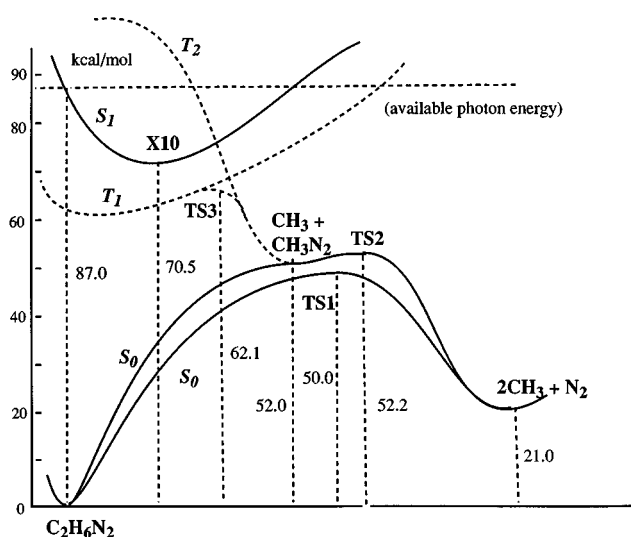


FIG. 11. Schematic overall potential energy profile of 350 nm photodissociation of *trans*-azomethane.

toward *cis*-azomethane, not directly toward dissociation, the system is expected to stay as a vibrationally excited molecule for a while. This suggests a statistical behavior of the system at this stage. Then the system can take either the sequential dissociation pathway to  $\text{CH}_3\text{N}_2 + \text{CH}_3$  or the simultaneous dissociation pathway to **TS1**. If the choice is made statistically, the sequential pathway would be preferred. The phase space available for the sequential pathway is larger than that for the simultaneous pathway, as has been illustrated in a preceding section with a larger entropy for thermal dissociation for the former pathway. In the sequential pathway, the system will dissociate endoergically one of the C–N bonds to give the  $\text{CH}_3\text{N}_2$  intermediate. Of 87 kcal/mol of the photon energy, about 52 kcal/mol is used to climb over the endoergic barrier, and about 35 kcal/mol is distributed into translational and internal energy of the first  $\text{CH}_3$  and the  $\text{CH}_3\text{N}_2$  fragment. Because of this barrier and the expected statistical behavior, it is not unreasonable to expect that the kinetic energy distribution is peaked at zero energy.<sup>35</sup> With this energy release, the  $\text{CH}_3\text{N}_2$  intermediate should dissociate very quickly over a very small activation energy of less than 1 kcal/mol. About 31 kcal/mol of the potential energy is released in this second stage. Since the barrier for this stage is very small, a large fraction of the released energy is expected to become the translational energy of the fragments.

The present proposed mechanism and calculated energetics are consistent with the recent experimental observations and can explain the two seemingly contradictory experiments.<sup>11–14</sup> In the favored sequential decomposition, two methyl fragments are formed at two different stages of reaction in different chemical environments. Thus, the translational and internal energy profiles would be different between the two fragments. However, the calculated activation barrier for the second step is so small that the methyldiazenyl radical should decompose immediately after its formation. This predicted short lifetime of methyldiazenyl is consistent

with the experimental result that the angles between the asymptotic center-of-mass velocities for all three fragments are strongly correlated. One may say that the reaction is highly *asynchronous* but is nearly *concerted*, i.e., the two methyl radicals produced at different stages of the reaction but within a short time.

Our calculation suggests an existence of a statistically less favorable simultaneous dissociation pathway. In this pathway, two methyl fragments are dissociated at the same time via a symmetric transition state. Dynamically these two methyls are not required to have the same internal energy, but statistically they are likely to show a similar internal energy distribution. Though we have not evaluated the branching ratio, a small fraction of the reaction may follow this pathway. It may be worth looking for such a process experimentally.

Another possible pathway is the involvement of a triplet state.<sup>16</sup> As seen in Fig. 11, the  $T_2$  state crossed with the  $S_1$  state within the available energy and correlates diabatically to the intermediate  $\text{CH}_3\text{N}_2 + \text{CH}_3$ . More theoretical studies on dynamics of the photodissociation process including not only  $S_0$  and  $S_1$  potential surfaces but also  $T_1$  and  $T_2$  potential surfaces would be needed to understand which of the possible pathways is dominant.

#### IV. CONCLUSIONS

(1) Results of high level *ab initio* calculations indicate that the ordering of electronic states of *trans*-azomethane at the Franck–Condon region is (in increasing energy order)  $S_0$ ,  $T_1$ ,  $S_1$ ,  $T_2$ ,  $T_3$ ,  $S_2$ , and  $S_3$ . Experimental assignment of 350 nm photoexcitation to the  $S_0 \rightarrow S_1$  transition was confirmed by the calculated vertical excitation energies. In all the regions we explored, the  $T_2$  surface is above  $S_1$ , and  $T_1$  is below but closely parallel to  $S_1$ . Electronic states relevant to 350 nm photochemistry of azomethane are identified to be  $S_1$  and  $S_0$ , as the singlet  $\rightarrow$  triplet transition and singlet  $\rightarrow$  triplet intersystem crossing are spin forbidden, and therefore must be very slow.

(2) Starting from the Franck–Condon region (CNNC dihedral angle of  $180^\circ$ ), decreasing the CNNC dihedral angle toward the perpendicular structure lowers the energy of the  $S_1$  state and increases the energy of the  $S_0$  state, thus bringing the two surfaces together. These two surfaces cross around the perpendicular nuclear configuration. The structure of the lowest point on the crossing seam is found by sa-CASSCF(6,4)/DZP to be asymmetrical with a CNNC dihedral angle of  $93^\circ$ . At MRCISD(Q)/DZP level of theory, the lowest crossing point is 18 kcal/mol lower than the  $S_0 \rightarrow S_1$  vertical excitation energy, and this crossing seam is easily accessible to the excited molecules and fast internal conversion is expected to bring the excited molecules back to the ground state efficiently.

(3) Starting with the lowest point on the seam of crossing, IRC calculations on the ground-state potential surface lead to *cis*-azomethane, indicating that 350 nm photoexcitation of *trans*-azomethane results in *cis*–*trans* isomerization in the condensed phase. In the gas phase, molecules carrying

photon energies can not be effectively deactivated by collision, and the trajectory will sat in the molecular region for a while and find a way to the C–N bond dissociation on the ground-state potential surface.

(4) The transition state structure of the simultaneous C–N bond cleavage of *trans*-azomethane was located by both MP2 and CASSCF methods. Vibrational analyses indicate it is a genuine transition state with only one imaginary mode, the symmetric C–N stretching. The first step of the sequential mechanism was found to be direct dissociation of the C–N bond without a transition structure at all levels of theory, resulting in methyldiazenyl and methyl radicals. Dissociation of the second C–N has an activation barrier of less than 1 kcal/mol, indicating methyldiazenyl has a very short lifetime. At the highest level of theory, the overall activation energy of the sequential mechanism is 7 kcal/mol higher than that of the simultaneous mechanism, but the sequential mechanism is strongly favored by reaction entropy. The calculations predict that as the temperature is above 0 °C, the free energy of activation of the sequential decomposition is lower than the simultaneous mechanism.

(5) Photodissociation is expected to take place sequentially as well. In the sequential mechanism, dissociation of the first C–N bond on the  $S_0$  surface takes place endoergically without reverse barrier resulting in  $\text{CH}_3\text{N}_2$  intermediates, which decompose almost immediately over a barrier of less than 1 kcal/mol. Thus the photodissociation reaction is highly asynchronous but is nearly concerted. This mechanism can explain two seemingly contradictory photodissociation experiments that two methyl radicals have very different translational as well as internal energies and that the velocity vectors of the three fragments are strongly correlated. There is also a statistically unfavorable simultaneous dissociation pathway, which may be worth searching experimentally.

The dynamic speculation we have made, based on the potential energy characteristics in the present paper, would require further confirmation. Any classical or quantum dynamics calculation would be desirable, if one can obtain reasonable potential functions.

## ACKNOWLEDGMENTS

The authors are grateful to Professor Y. T. Lee and Dr. Allan Bracker for discussion and communication, Professor Weisman for discussion, and Professor E. Weitz for a preprint. The present research is in part supported by a grant F49620-95-1-0182 from the Air Force Office of Scientific Research.

<sup>1</sup>P. S. Engel, *Chem. Rev.* **80**, 99 (1980).

<sup>2</sup>P. S. Engel and C. Steel, *Acc. Chem. Res.* **6**, 275 (1973).

<sup>3</sup>J. G. Calvert and J. N. Pitts, *Photochemistry* (Wiley, New York, 1967).

<sup>4</sup>S. S. Collier, D. H. Slater, and J. G. Calvert, *Photochem. Photobiol.* **7**, 737 (1968).

<sup>5</sup>M. B. Robin, B. R. Hart, and N. A. Kuebler, *J. Am. Chem. Soc.* **89**, 1564 (1967).

<sup>6</sup>O. A. Mosher, M. S. Foster, W. M. Flicker, J. L. Beauchamp, and A. Kuppermann, *J. Chem. Phys.* **62**, 3424 (1975).

<sup>7</sup>C. V. Cannon and O. K. Rice, *J. Am. Chem. Soc.* **63**, 2900 (1941).

<sup>8</sup>M. H. Jones and E. W. R. Steacie, *J. Chem. Phys.* **21**, 1018 (1953).

<sup>9</sup>H. C. Ramsperger, *J. Am. Chem. Soc.* **49**, 912 (1927).

<sup>10</sup>H. C. Ramsperger, *J. Am. Chem. Soc.* **51**, 2134 (1929).

<sup>11</sup>P. L. Holt, K. E. McCurdy, J. S. Adams, K. A. Burton, R. B. Weisman, and P. S. Engel, *J. Am. Chem. Soc.* **107**, 2180 (1985).

<sup>12</sup>K. A. Burton and R. B. Weisman, *J. Am. Chem. Soc.* **112**, 1804 (1990); B. K. Andrews, K. A. Burton, and R. B. Weisman, *J. Chem. Phys.* **96**, 1111 (1992).

<sup>13</sup>S. W. North, C. A. Longfellow, and Y. T. Lee, *J. Chem. Phys.* **99**, 4423 (1993); S. W. North, D. A. Black, J. D. Gezelter, C. A. Longfellow, and Y. T. Lee, *ibid.* **102**, 4447 (1995).

<sup>14</sup>D. H. Fiarbrother, K. A. Dickens, P. C. Stair, and E. Weitz, *Chem. Phys. Lett.* **246**, 513 (1995).

<sup>15</sup>R. N. Camp, I. R. Epstein, and C. Steel, *J. Am. Chem. Soc.* **99**, 2453 (1977).

<sup>16</sup>J. Metcalfe, S. Chervinsky, and I. Oref, *Chem. Phys. Lett.* **42**, 190 (1976).

<sup>17</sup>R. Liu and K. Morokuma, *Ab initio* Study of 350 nm Photodissociation Mechanism of Azomethane, presented at 23rd Southeastern Theoretical Chemistry Association Conference, Nashville, TN, May 20–21, 1994.

<sup>18</sup>(a) C.-H. Hu and H. F. Schaefer III, *J. Chem. Phys.* **101**, 1289 (1994); (b) *J. Phys. Chem.* **99**, 7507 (1995).

<sup>19</sup>(a) B. K. Andrews and R. B. Weisman, *J. Chem. Phys.* **101**, 6776 (1994); (b) B. K. Andrews, Ph.D. thesis, Rice University, 1992.

<sup>20</sup>H.-J. Werner and P. J. Knowles, *J. Chem. Phys.* **82**, 5053 (1985); P. J. Knowles and H.-J. Werner, *Chem. Phys. Lett.* **115**, 259 (1985).

<sup>21</sup>T. H. Dunning Jr., *J. Chem. Phys.* **53**, 2823 (1970).

<sup>22</sup>H.-J. Werner and W. Meyer, *J. Chem. Phys.* **73**, 2342 (1980); **74**, 5794 (1981).

<sup>23</sup>H.-J. Werner and P. J. Knowles, *J. Chem. Phys.* **89**, 5803 (1988); P. J. Knowles and H.-J. Werner, *Chem. Phys. Lett.* **145**, 514 (1988).

<sup>24</sup>T. H. Dunning Jr., *J. Chem. Phys.* **90**, 1007 (1989).

<sup>25</sup>W. J. Hehre, R. D. Ditchfield, and J. A. Pople, *J. Chem. Phys.* **56**, 2257 (1972).

<sup>26</sup>R. Krishnan, M. J. Frisch, and J. A. Pople, *J. Chem. Phys.* **72**, 4244 (1980).

<sup>27</sup>GAUSSIAN 92, Revision A, M. J. Frisch, G. W. Trucks, M. Head-Gordon, P. M. W. Gill, M. W. Wong, J. B. Foresman, B. G. Johnson, H. B. Schlegel, M. A. Robb, E. S. Replogle, R. Gomperts, J. L. Andres, K. Raghavachari, J. S. Binkley, C. Gonzalez, R. L. Martin, D. J. Fox, D. J. Defrees, J. Baker, J. J. P. Stewart, and J. A. Pople (Gaussian, Inc., Pittsburgh, PA 1992); GAUSSIAN 94, Revision A.1, M. J. Frisch, G. W. Trucks, H. B. Schlegel, P. M. W. Gill, B. G. Johnson, M. A. Robb, J. R. Cheeseman, T. Keith, G. A. Petersson, J. A. Montgomery, K. Raghavachari, M. A. Al-Laham, V. G. Zakrzewski, J. V. Ortiz, J. B. Foresman, J. Cioslowski, B. B. Stefanov, A. Nanayakkara, M. Challacombe, C. Y. Peng, P. Y. Ayala, W. Chen, M. W. Wong, J. L. Andres, E. S. Replogle, R. Gomperts, R. L. Martin, D. J. Fox, J. S. Binkley, D. J. Defrees, J. Baker, J. P. Stewart, M. Head-Gordon, C. Gonzalez, and J. A. Pople, Gaussian, Inc., Pittsburgh PA, 1995.

<sup>28</sup>MOLPRO, H.-J. Werner and P. J. Knowles (University of Sussex, 1991).

<sup>29</sup>Reference 3, p. 453.

<sup>30</sup>E. Haselbach and E. Heibronner, *Helv. Chem. Acta* **53**, 684 (1970).

<sup>31</sup>E. Haselbach and S. Schmelzer, *Helv. Chem. Acta* **54**, 1575 (1971); **55**, 1745 (1972).

<sup>32</sup>C. R. Brundle, M. B. Robin, N. S. Kuebler, and H. Basch, *J. Am. Chem. Soc.* **94**, 1451 (1972).

<sup>33</sup>K. N. Houk, Y.-M. Chang, and P. S. Engel, *J. Am. Chem. Soc.* **97**, 1824 (1975).

<sup>34</sup>C. Steel and A. F. Trotman, *J. Chem. Soc.* **1959**, 975.

<sup>35</sup>A. Bracker, S. W. North, and Y. T. Lee, presented at the 1995 Conference on the Dynamics of Molecular Collisions, Asilmare, CA, July 16–21, 1995.